Molecular modeling of inelastic electron transport in molecular junctions

2008 J. Phys.: Condens. Matter 20 374110

(http://iopscience.iop.org/0953-8984/20/37/374110)

IOP PUBLISHING JOURNAL OF PHYSICS: CONDENSED MATTER

J. Phys.: Condens. Matter **20** (2008) 374110 (12pp) doi:10.1088/0953-8984/20/37/374110

Molecular modeling of inelastic electron transport in molecular junctions

Jun Jiang, Mathias Kula and Yi Luo[1]

Department of Theoretical Chemistry, School of Biotechnology,
Royal Institute of Technology, S-106 91 Stockholm, Sweden

E-mail: luo@kth.se

Received 13 February 2008
Published 26 August 2008
Online at stacks.iop.org/JPhysCM/20/374110

Abstract

A quantum chemical approach for the modeling of inelastic electron tunneling spectroscopy of molecular junctions based on scattering theory is presented. Within a harmonic approximation, the proposed method allows us to calculate the electron–vibration coupling strength analytically, which makes it applicable to many different systems. The calculated inelastic electron transport spectra are often in very good agreement with their experimental counterparts, allowing the revelation of detailed information about molecular conformations inside the junction, molecule–metal contact structures, and intermolecular interaction that is largely inaccessible experimentally.

(Some figures in this article are in colour only in the electronic version)

1. Introduction

The possibility of using single molecules to build electronic devices has attracted much attention in recent decades [1–12]. Many exciting developments have been made in the field in terms of technological advances and in-depth understanding of electron transport in molecules. However, one of the major bottlenecks in the field of molecular electronics is the lack of precise control of the molecule and metal contact, which sometimes even makes it difficult to prove the actual existence of real molecules in a junction. In this context, the development of inelastic electron tunneling spectroscopy (IETS) has been particularly useful. Inelastic electron tunneling (IET) is induced by the coupling of electron and nuclear motions in molecules. It is thus sensitive to molecular conformation, molecule–electrode bonding, and the environment. Moreover, the IET process is also strongly associated with molecular energetics, molecular dynamics, charge transfer, and chemical reactions. A good understanding of IET is of great importance for both fundamental physics and technical applications. IETS was developed in the 1960s to study the vibrational spectra of organic molecules buried inside metal–oxide–metal junctions. It has only recently become possible to apply it to single molecular junctions [13, 14], and been the subject of extensive experimental [13–24] and theoretical [25–38] studies.

[1] Author to whom any correspondence should be addressed.

We have developed a quantum chemical approach based on scattering theory that allows us to calculate the IETS of molecular junctions analytically within a harmonic approximation [31, 32]. Here, we will extend our approach to include the effect of thermal populations and to provide spatial distribution of vibration modes observed in IETS. We will demonstrate how the theoretical simulations can help to identify molecules, to determine molecular conformations and molecule–metal bonding, and to reveal intermolecular interactions in molecular junctions.

2. General theory

2.1. Molecular junctions

A typical molecular junction constitutes a molecule (M) sandwiched between two electron reservoirs, the source (S) and the drain (D), as schematically shown in figure 1(a). In most cases, reservoirs are made of metal contacts and the molecules could be either physically adsorbed or chemically bonded to the metal surface. It is difficult to consider the whole metal electrode in the quantum chemical simulations. But in reality, only an ‘extended molecule’ that covers the entire scattering region is needed for theoretical investigations. The size of the metal clusters making up the extended molecule is of course a matter that deserves to be extensively discussed. However, in the case of IETS, the most useful information comes from

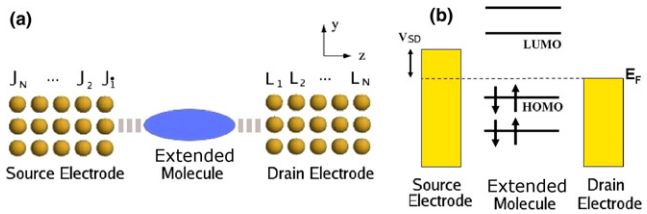

Figure 1. (a) Schematic drawing of a molecular junction. (b) Electronic structure of the extended molecule with respect to the Fermi distribution of the electrodes.

the molecular parts. Relatively small metal clusters could be used which can simplify the calculations significantly. In our simulations, we often use a cluster of three gold atoms, not as a matter of principle but because of limitations of computational capacity. The electronic structure of the extended molecule can be calculated with density functional theory, while the rest of the electrode is described by the effect mass approximation. A schematic energy diagram of the source–extended molecule–drain system is given in figure 1(b), to elucidate the basic physics of the electron transport process.

Under an external bias, Fermi energy in the source is shifted up or down with respect to that of the drain. Due to different Fermi populations, free electrons in the source reservoir inject to the extended molecule, tunnel to the drain electrode, and form an electron current. The whole process is dominated by electrons scattering through different scattering channels, which are the molecular orbitals in the extended molecule. The primary part of the current comes from the electron elastic tunneling process and is free from the electron–phonon coupling effect. On the other hand, if the injected electron has energy coupled with a certain vibrational mode, the tunneling process can be strongly affected by the nuclear motion. In that case, IET occurs and induces normally small changes to the primary current–voltage (I–V) characteristics.

2.2. Elastic electron transport

There are many different approaches available in the literature [3, 4]. Most of them are based on solid state physics, which follow naturally from its success in semiconductors [8–11]. A bottom-up approach is also developed using quantum chemical methods that are particularly useful for electronic structures of molecular systems. The Green's function formulation developed by Mujica *et al* [12] is a good starting point for the quantum chemical based methods. Along this line, several attempts [39–41] have been made to study the transmission probability of molecular junctions. We have also developed a simple yet versatile quantum chemical method for simulations of electron tunneling in molecular junctions which will be briefly described here.

The Born–Oppenheimer (BO) approximation, as well as the one-particle approximation, has been adopted in the model. For a typical molecular junction shown in figure 1(a), the corresponding one-particle Hamiltonian, H, can be represented in a matrix format as

$$H = \begin{pmatrix} H^{\mathrm{SS}} & U^{\mathrm{SM}} & U^{\mathrm{SD}} \\ U^{\mathrm{MS}} & H^{\mathrm{MM}} & U^{\mathrm{MD}} \\ U^{\mathrm{DS}} & U^{\mathrm{DM}} & H^{\mathrm{DD}} \end{pmatrix} \tag{1}$$

where $H^{\mathrm{SS,DD,MM}}$ are the Hamiltonians of subsystems S, D and M, respectively. U is the interaction between or among subsystems. Using the same principle, the eigenstate Ψ^η at energy level ε_η can be partitioned into three parts:

$$\begin{aligned}
|\Psi^\eta\rangle &= |\Psi^{\eta,\mathrm{S}}\rangle + |\Psi^{\eta,\mathrm{M}}\rangle + |\Psi^{\eta,\mathrm{D}}\rangle \\
|\Psi^{\eta,\mathrm{S}}\rangle &= \sum a_i^{\eta,\mathrm{S}} |\phi_i^{\mathrm{S}}\rangle \\
&= \sum_J^{J_N} \left(\sum_i a_i^{\eta,J} |\phi_i^J\rangle \right) = \sum_J^{J_N} |J^\eta\rangle \\
|\Psi^{\eta,\mathrm{M}}\rangle &= \sum a_i^{\eta,\mathrm{M}} |\phi_i^{\mathrm{M}}\rangle \\
&= \sum_K^{K_N} \left(\sum_i a_i^{\eta,K} |\phi_i^K\rangle \right) = \sum_K^{K_N} |K^\eta\rangle \\
|\Psi^{\eta,\mathrm{D}}\rangle &= \sum a_i^{\eta,D} |\phi_i^{\mathrm{D}}\rangle \\
&= \sum_L^{L_N} \left(\sum_i a_i^{\eta,L} |\phi_i^L\rangle \right) = \sum_L^{L_N} |L^\eta\rangle
\end{aligned} \tag{2}$$

where $\Psi^{\mathrm{S,D,M}}$ and $\phi_i^{\mathrm{S,D,M}}$ are the wavefunction and basis function of subsystems S, D and M, respectively. Here J, K and L runs over the atomic sites in the extended molecule.

The interaction at energy level ε_η can be written as

$$\begin{aligned}
U^\eta = &\sum_{J,K} V_{JK} |J^\eta\rangle\langle K^\eta| + \sum_{K,J} V_{KJ} |K^\eta\rangle\langle J^\eta| \\
&+ \sum_{K',L} V_{K'L} |K'^\eta\rangle\langle L^\eta| + \sum_{L,K'} V_{LK'} |L^\eta\rangle\langle K'^\eta| \\
&+ \sum_{J',J} V_{J'J} |J'^\eta\rangle\langle J^\eta| + \sum_{L,L'} V_{LL'} |L^\eta\rangle\langle L'^\eta| \\
&+ \sum_{J,L} V_{JL} |J^\eta\rangle\langle L^\eta| + \sum_{L,J} V_{LJ} |L^\eta\rangle\langle J^\eta|
\end{aligned} \tag{3}$$

where V_{AB} represents the coupling energy between sites A and B, which can be calculated analytically with quantum chemical methods using the following expression:

$$V_{AB} = \sum_\nu^{\mathrm{OCC}} \langle A^\nu | H | B^\nu \rangle = \sum_\nu^{\mathrm{OCC}} \sum_{A_i,B_i} a_{A_i}^\nu a_{B_i}^\nu \langle \phi_{A_i} | H | \phi_{B_i} \rangle \tag{4}$$

where $\langle \phi_{A_i} | H | \phi_{B_i} \rangle = F_{A_i,B_i}$ is the interaction energy between two atomic basis functions.

Based on the elastic-scattering Green's function theory, the transition operator is defined as

$$T = U + UGU \tag{5}$$

where G is the Green's function: $G(z) = (z - H)^{-1}$.

For an electron scattering from the initial sites $\sum |J'\rangle$ of reservoirs S to the final sites $\sum |L'\rangle$ of reservoirs D (where J' and L' run over the atomic site of the source and the drain electrode, respectively), the transition probability is the

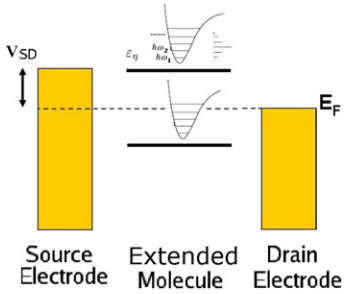

Figure 2. Schematic drawing of electron–vibration coupling in a molecular junction.

summation of transition matrix elements through all the energy levels and reservoir sites:

$$T = \left| \sum_{\eta} \sum_{J',L'} T^{\eta}_{J'L'} \right|^2 \tag{6}$$

in which the transition matrix element is

$$T^{\eta}_{J'L'} = \langle J'|U|L'\rangle + \langle J'|UGU|L'\rangle. \tag{7}$$

Thus, substituting U^{η} of equation (3) into equation (7) and taking into account the fact that there is no direct coupling between two reservoirs, we obtained

$$T^{\eta}_{J'L'} = \sum_{K,K'} V_{J'K'} \langle K'^{\eta}| \frac{1}{z-H} |K^{\eta}\rangle V_{KL'} \tag{8}$$

where the parameter z in the Green's function is a complex variable, $z = E_i + \mathrm{i}\Gamma_i$, and E_i is the energy at which the scattering process is observed. Due to the energy conservation rule, the incoming and outgoing electrons should have the same energy, i.e. belong to the same orbital. In an elastic-scattering process, E_i equals the energy of the tunneling electron when it enters the scattering region from the reservoir S, as well as the energy at which the electron is collected at time $+\infty$ by the reservoir D. $1/\Gamma_i$ is the escape rate, which is determined by the Fermi golden rule [42].

2.3. Inelastic electron transport

In the electron tunneling process, if the electron crossing the junction is able to exchange a definite amount of energy with the molecular nuclear motion, an inelastic component will contribute to the electron current. In figure 2, one can see that the molecular orbitals are coupled to the vibrational normal modes, which then serve as individual scattering channels for the IET process. In other words, one should be able to observe vibration modes of the molecular systems in conductivity measurements.

In the adiabatic Born–Oppenheimer approximation, the electronic Hamiltonian of a molecular system can be considered parametrically as a function of vibrational normal modes Q. The Schrödinger equation could be written as

$$\begin{aligned} &H(Q,e)|\Psi^{\eta}(Q,e)\rangle|\Psi^{\nu}(Q)\rangle \\ &= \left(\varepsilon_{\eta} + \sum_{a} n^{\nu}_{a}\hbar\omega_{a}\right)|\Psi^{\eta}(Q,e)\rangle|\Psi^{\nu}(Q)\rangle \end{aligned} \tag{9}$$

where $H(Q,e)$ is the electronic and the vibrational Hamiltonian, ε_{η} represents the energy of eigenstate η of the pure electronic Hamiltonian, ω_a is the vibrational frequency of vibrational normal modes Q_a and n^{ν}_{a} is the quantum number for the mode Q_a in $|\Psi^{\nu}(Q)\rangle$.

By using a Taylor expansion, the nuclear motion dependent wavefunction can be expanded along each vibrational normal mode. With the help of adiabatic harmonic approximation, we can then use the first derivative like $\frac{\partial\Psi(Q)}{\partial Q_a}$ to represent the vibrational motion part in the wavefunctions [25]. Therefore, the vibration dependent wavefunction of an eigenstate ε_{η} becomes

$$\begin{aligned} &|\Psi^{\eta}(Q,e)\rangle|\Psi^{\nu}(Q)\rangle \\ &= \left|\Psi^{\eta}_{0|Q=0} + \sum_{a} \frac{\partial\Psi^{\eta}_{0}}{\partial Q_a} Q_{a|Q=0} + \cdots\right\rangle |\Psi^{\nu}(Q)\rangle \end{aligned} \tag{10}$$

where $|\Psi^{\nu}(Q)\rangle$ is the vibration wavefunction. Ψ^{η}_{0} is here the intrinsic electronic wavefunction at the equilibrium position, Q_0.

Since electrodes in a molecular junction are always composed of large numbers of metal atoms, the vibronic information of electrodes smears out in the free-electron atmosphere. Thus, it is normally assumed that the electron–vibronic coupling is important only for the extended molecule part [43]. The site representation of the vibration dependent wavefunction for the source, extended molecule, and drain is

$$\begin{aligned} &|\Psi^{\eta}(Q,e)\rangle|\Psi^{\nu}(Q)\rangle = (|\Psi^{\eta,\mathrm{S}}(Q,e)\rangle + |\Psi^{\eta,\mathrm{M}}(Q,e)\rangle \\ &\quad + |\Psi^{\eta,\mathrm{D}}(Q,e)\rangle)|\Psi^{\nu}(Q)\rangle \\ &|\Psi^{\eta,\mathrm{S}}(Q,e)\rangle|\Psi^{\nu}(Q)\rangle = \sum_{J}^{J_N} |J^{\eta}(Q,e)\rangle|\Psi^{\nu}(Q)\rangle \\ &= \sum_{J}^{J_N} |J^{\eta}_{0|Q=0}\rangle|\Psi^{\nu}(Q)\rangle \\ &|\Psi^{\eta,\mathrm{M}}(Q,e)\rangle|\Psi^{\nu}(Q)\rangle = \sum_{K}^{K_N} |K^{\eta}(Q,e)\rangle|\Psi^{\nu}(Q)\rangle \\ &= \sum_{K}^{K_N} \left|K^{\eta}_{0|Q=0} + \sum_{a} \frac{\partial K^{\eta}_{0}}{\partial Q_a} Q_{a|Q=0} + \cdots\right\rangle |\Psi^{\nu}(Q)\rangle \\ &|\Psi^{\eta,\mathrm{D}}(Q,e)\rangle|\Psi^{\nu}(Q)\rangle = \sum_{L}^{L_N} |L^{\eta}(Q,e)\rangle|\Psi^{\nu}(Q)\rangle \\ &= \sum_{L}^{L_N} |L^{\eta}_{0|Q=0}\rangle|\Psi^{\nu}(Q)\rangle. \end{aligned} \tag{11}$$

With the newly defined vibronic dependent Hamiltonian and wavefunction we can rewrite the transition matrix element as given in equation (8) by using vibronic dependent wavefunctions.

$$\begin{aligned} T^{\eta}_{J'L'}(Q) &= \sum_{K,K'} \sum_{\nu'\nu} V_{J'K'}(Q)_{|Q=0} \langle\Psi^{\nu'}(Q)|\langle K'^{\eta}(Q,e)| \\ &\quad \times \frac{1}{z - H(Q,e)} |K^{\eta}(Q,e)\rangle|\Psi^{\nu}(Q)\rangle V_{KL'}(Q)_{|Q=0} \\ &= \sum_{K,K'} V_{J'K'}(Q)_{|Q=0} V_{KL'}(Q)_{|Q=0} \end{aligned}$$

$$\times \sum_{\nu',\nu,\nu''} \langle \Psi^{\nu'}(Q)|\langle K'^{\eta}(Q,e)|\frac{1}{z_\eta - H(Q,e)}|\Psi^{\eta,\nu''}(Q)\rangle$$
$$\times \langle \Psi^{\eta,\nu''}(Q)|K^{\eta}(Q,e)\rangle|\Psi^{\nu}(Q)\rangle$$
$$= \sum_{K,K'} V_{J'K'}(Q)_{|Q=0} V_{KL'}(Q)_{|Q=0} \sum_{\nu',\nu,\nu''} g^{\eta,\nu',\nu,\nu''}_{KK'}. \quad (12)$$

Applying the vibrational normal mode theory, we have

$$g^{\eta,\nu',\nu,\nu''}_{KK'} = \langle \Psi^{\nu'}(Q)|\langle K'^{\eta}(Q,e)|\frac{1}{z_\eta - H(Q,e)}|\Psi^{\eta,\nu''}(Q)\rangle$$
$$\times \langle \Psi^{\eta,\nu''}(Q) \mid K^{\eta}(Q,e)\rangle|\Psi^{\nu}(Q)\rangle$$
$$= \{\langle \Psi^{\nu'}(Q)|\langle K'^{\eta}(Q,e) \mid \Psi^{\eta}(Q,e)\rangle|\Psi^{\nu''}(Q)\rangle$$
$$\times \langle \Psi^{\nu''}(Q)|\langle \Psi^{\eta}(Q,e) \mid K^{\eta}(Q,e)\rangle|\Psi^{\nu}(Q)\rangle\}$$
$$\times \left\{ z_\eta - \varepsilon_\eta - \sum_a n_a^{\nu''}\hbar\omega_a \right\}^{-1}. \quad (13)$$

Therefore, with Taylor expansion, $g^{\eta,\nu',\nu,\nu''}_{K'K}$ can be computed through

$$g^{\eta,\nu',\nu,\nu''}_{K'K} = \frac{1}{z_\eta - \varepsilon_\eta - \sum_a n_a^{\nu''}\hbar\omega_a}\left[\left\langle K_0'^{\eta}\right| \sum_a \frac{\partial \Psi_0^{\eta}}{\partial Q_a} Q_a^{\nu'\nu''}\right\rangle$$
$$+ \left\langle \sum_a \frac{\partial K_0'^{\eta}}{\partial Q_a} Q_a^{\nu'\nu''}\middle|\Psi_0^{\eta}\right\rangle\left]\left[\left\langle K_0^{\eta}\right| \sum_a \frac{\partial \Psi_0^{\eta}}{\partial Q_a} Q_a^{\nu''\nu}\right\rangle\right.$$
$$+ \left\langle \sum_a \frac{\partial K_0^{\eta}}{\partial Q_a} Q_a^{\nu''\nu}\middle|\Psi_0^{\eta}\right\rangle\right]. \quad (14)$$

Since most of the IET signals are measured at low temperature, we can assume that only the ground vibrational state is populated. With harmonic approximation, we have

$$Q_a^{\nu'\nu''} = \langle \nu'|Q_a|\nu''\rangle = \langle 0|Q_a|1\rangle = \sqrt{\frac{\hbar}{2\omega_a}}. \quad (15)$$

And the total transmission becomes

$$\sum_{\nu',\nu,\nu''} g^{\eta,\nu',\nu,\nu''}_{K'K} = \sum_a \frac{1}{z_\eta - \varepsilon_\eta - \hbar\omega_a} \times \sqrt{\frac{\hbar}{2\omega_a}}\left[\left\langle K_0'^{\eta}\middle|\frac{\partial \Psi_0^{\eta}}{\partial Q_a}\right\rangle\right.$$
$$\left.+ \left\langle \frac{\partial K_0'^{\eta}}{\partial Q_a}\middle|\Psi_0^{\eta}\right\rangle\right]\left[\left\langle K_0^{\eta}\middle|\frac{\partial \Psi_0^{\eta}}{\partial Q_a}\right\rangle + \left\langle \frac{\partial K_0^{\eta}}{\partial Q_a}\middle|\Psi_0^{\eta}\right\rangle\right]. \quad (16)$$

The inclusion of nuclear motion introduces vibrational excited states in the electronic ground state potential. These vibrational excited states are the ones that contribute to the inelastic terms in the case of off-resonant excitation. Meanwhile, the electron can also tunnel through the molecular orbitals, resulting in the elastic term in the total current.

2.4. Thermal population

At low temperature, only the ground vibrational state is populated. This assumption works very well for molecular systems since their vibrational frequencies are considerably large. However, in the case of molecular junctions the coupling modes between the molecule and the electrodes can have very small vibrational frequencies, which make it possible for them to be populated even at quite low energy. The effect of thermal population on IETS should thus be examined.

Starting from equation (14) in the previous section, we rewrite the equation (15) for the vibronic operator:

$$Q_a^{\nu'\nu''} = \langle \nu'|Q_a|\nu''\rangle$$
$$= \sqrt{\frac{\hbar}{2\omega_a}}\left(\sqrt{n_a^{\nu'}+1}\langle n_a^{\nu'}+1 \mid n_a^{\nu''}\rangle\right.$$
$$\left.+ \sqrt{n_a^{\nu'}}\langle n_a^{\nu'}-1 \mid n_a^{\nu''}\rangle\right). \quad (17)$$

With the harmonic approximation, transitions between $|\nu\rangle$ to $|\nu \pm 1\rangle$ are possible. For a function linearly depending on $Q_a^{\nu'\nu''}$, we have

$$\sum_{\nu'} f[Q_a^{\nu'\nu''}] = f\left[\sqrt{\frac{\hbar}{2\omega_a}}\left(\sqrt{n_a^{\nu''}}\langle n_a^{\nu''}-1 \mid n_a^{\nu''}-1\rangle\right.\right.$$
$$\left.\left.+ \sqrt{n_a^{\nu''}+1}\langle n_a^{\nu''} \mid n_a^{\nu''}\rangle\right)\right]$$
$$= f\left[\sqrt{\frac{\hbar}{2\omega_a}}\left(\sqrt{n_a^{\nu''}}P_{n_a^{\nu''}-1} + \sqrt{n_a^{\nu''}+1}P_{n_a^{\nu''}}\right)\right]$$
$$= f[R_a^{\nu''}] \quad (18)$$

where $P_{n_a^{\nu''}}$ is the thermal population of state $|n_a^{\nu''}\rangle$, and can be approximated to be the Boltzmann distribution as $e^{-[\Delta E/k_B T]}$, in which ΔE is the energy difference between the eigenenergies of states 0 and $|n_a^{\nu''}\rangle$, k_B is the Boltzmann constant; T is the temperature. Equation (16) can thus be rewritten as

$$\sum_{\nu',\nu,\nu''} g^{\eta,\nu',\nu,\nu''}_{K'K} = \sum_{\nu''} \frac{1}{z_\eta - \varepsilon_\eta - \sum_a n_a^{\nu''}\hbar\omega_a}$$
$$\times \left[\left\langle K_0'^{\eta}\middle| \sum_a \frac{\partial \Psi_0^{\eta}}{\partial Q_a} R_a^{\nu''}\right\rangle + \left\langle \sum_a \frac{\partial K_0'^{\eta}}{\partial Q_a} R_a^{\nu''}\middle|\Psi_0^{\eta}\right\rangle\right]$$
$$\times \left[\left\langle K_0^{\eta}\middle| \sum_a \frac{\partial \Psi_0^{\eta}}{\partial Q_a} R_a^{\nu''}\right\rangle + \left\langle \sum_a \frac{\partial K_0^{\eta}}{\partial Q_a} R_a^{\nu''}\middle|\Psi_0^{\eta}\right\rangle\right]. \quad (19)$$

Because of the exponential decay of the Boltzmann distribution, vibrational states with high frequencies and high quantum numbers will make negligible contributions to the IETS, which simplifies the calculations.

2.5. Electron current

Based on the Landauer formula [44], electron current through a molecular wire can be computed by integrating the transition probability over all energy states in the reservoir. The molecule is assumed to be aligned along the z direction in figure 1, which is also the direction of current flow. Within the effective mass approximation, energy states in the conduction band of the reservoir can be expressed as the summation, $E = E_{x,y} + E_z + E_c$, where E_c is the conduction band edge and is used as energy reference. It is assumed that the parabolic dispersion relation for the energy states in metal holds. The electrons in the reservoir are assumed to be all in equilibrium at a temperature T and Fermi level E_f. When an applied voltage

V is introduced, the tunneling current density from source (S) to drain (D) is [12, 42, 45, 46]

$$i_{\mathrm{SD}} = \frac{2\pi e}{\hbar} \sum_{E_{x,y}} \sum_{E_z^l, E_z^{l'}} [f(E_{x,y} + E_z^l - eV) - f(E_{x,y} + E_z^{l'})] \times T_{l'l}\delta(E_z^{l'} - E_z^l) \tag{20}$$

where $f(E)$ is the Fermi distribution function,

$$f(E) = \frac{1}{\mathrm{e}^{[(E-E_{\mathrm{f}})/k_{\mathrm{B}}T]} + 1}.$$

Here k_{B} is the Boltzmann constant, T is the temperature and $T_{l'l}$ is the transition probability describing the scattering process from the initial state $|l\rangle$ to the final state $|l'\rangle$; this transition probability is a function of the quantized injection energies along the z-axis, E_z^l and $E_z^{l'}$.

For one-dimensional electron systems, the current through a molecular junction can be computed by the relationship: $I^{1\mathrm{D}} = i^{1\mathrm{D}}$. The current for a two-dimensional electron system follows $I^{2\mathrm{D}} = r_{2\mathrm{s}} i^{2\mathrm{D}}$, where $r_{2\mathrm{s}}$ is the effective injection length of the transmitting electron and is determined by the density of electrons $N_{2\mathrm{D}} \approx 1/(\pi r_{2\mathrm{D}}^2)$, which itself can be calculated as $N_{2\mathrm{D}} = (4\pi m^* E_{\mathrm{f}})/h^2$. For a three-dimensional system, the total conduction current is $I_{3\mathrm{D}} = A i_{3\mathrm{D}}$, where A is the effective injection area of the transmitting electron from the metal electrode, determined by the density of electronic states of the bulk metal. We have assumed that the effective injection area $A \approx \pi r_{3\mathrm{s}}^2$, where $r_{3\mathrm{s}}$ is defined as the radius of a sphere whose volume is equal to the volume per conduction electron, $r_{3\mathrm{s}} = (3/4\pi N_{3\mathrm{D}})^{1/3}$. $N_{3\mathrm{D}} = (2m^* E_{\mathrm{f}})^{3/2}/(3\hbar^3\pi^2)$ is here the density of electronic states of the bulk metal. By introducing the effective injection area, we have removed the complications related to the calculations of the self-energy [42]. The conductance g is obtained by

$$g = \frac{\partial I}{\partial V}. \tag{21}$$

The total current in molecular devices can be decomposed into two parts

$$I = I_{\mathrm{el}} + I_{\mathrm{inel}} \tag{22}$$

where I_{el} and I_{inel} are respectively the elastic and inelastic contributions to the electron tunneling current. Typically, only a fraction of tunneling electrons are involved in the IET process. The small conductance change induced by the electron–vibronic coupling is commonly measured by the second harmonics of a phase-sensitive detector for the second derivative of the tunneling current

$$\mathrm{d}^2 I/\mathrm{d}V^2$$

or the part normalized by the differential conductance

$$(\mathrm{d}^2 I/\mathrm{d}V^2)/(\mathrm{d}I/\mathrm{d}V).$$

2.6. Computational scheme

Our theoretical approach has been implemented into a portable program, called QCME (quantum chemistry for molecular electronics) [47]. The package can be easily applied to systems of different size. And it can be interfaced with existing quantum chemistry packages with desired computational methods. The modeling starts by setting up a proper computational model, i.e. define the extended molecular systems. In most studies presented here, the extended molecule consists of two triangular atomic clusters of three gold atoms and the molecule. The inclusion of small gold clusters is found to be adequate for modeling of IETS. The geometry, electronic structure, and vibrational normal modes of model system are calculated using one-particle approximation. The hybrid density functional theory (DFT), B3LYP [48], together with an effective core potential (ECP) basis set, LanL2DZ [49], have often been used in our studies. We have found that the electron transport properties of molecular junctions do not strongly depend on the choice of functionals. We have so far mainly used a Gaussian program for electronic structure calculations [50]. With the QCME program we obtain the coupling coefficients, transition matrix, I–V characteristics and IETS spectrum.

3. Results

We will present here several examples to show different aspects of IETS in molecular junctions and the importance of theoretical modeling.

3.1. Temperature dependence

IETS has so far been measured experimentally at very low temperatures. The change of temperature has drastic effects on the IET processes. According to our formulation, one can identify two major factors that are strongly associated with the temperature: (1) the thermal population of vibrational states, related to the Boltzmann distribution $P_{n_a^{\nu''}} = \mathrm{e}^{-[\Delta E/k_{\mathrm{B}}T]}$, and (2) the Fermi distribution of electron, $f(E) = \frac{1}{\mathrm{e}^{[(E-E_{\mathrm{f}})/k_{\mathrm{B}}T]}+1}$ and $f(E) = \frac{1}{\mathrm{e}^{[(E-E_{\mathrm{f}}-eV_{\mathrm{D}})/k_{\mathrm{B}}T]}+1}$. Both show exponential dependence on the temperature. In the case of Fermi distribution, the energy difference $E - E_{\mathrm{f}}$ and $E - E_{\mathrm{f}} - eV_{\mathrm{D}}$ can easily reach zero within the transport window. Hence, the Fermi distribution induced temperature effects can be constantly effective. The temperature effects on IETS caused by the Boltzmann distribution of the vibrational population can only be observed for vibrational modes with very small frequencies.

The temperature effect on IETS of an octane dithiol molecular junction was investigated in our previous study [31], where only the Fermi distribution was considered. Here we used the same computational model for the extended molecule Au_3–$S(CH_2)_8S$–Au_3 to include contributions from both the Fermi distribution and the thermal population. The calculated electron tunneling current (including both elastic and inelastic parts) is illustrated as a function of applied bias in figure 3(B), together with the corresponding experimental I–V curve of Wang *et al* [14] in figure 3(A). It is noted that the shape of

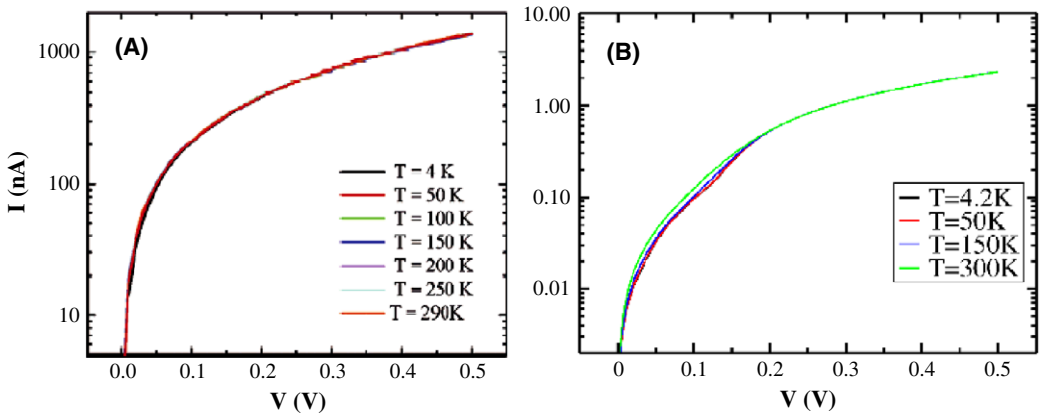

Figure 3. Current (on a log scale) of a gold–octane dithiol–gold junction as a function of voltage at different temperatures. (A) Experiments from Wang *et al* [14]. (B) Calculated total electron tunneling current (including both elastic and inelastic contributions).

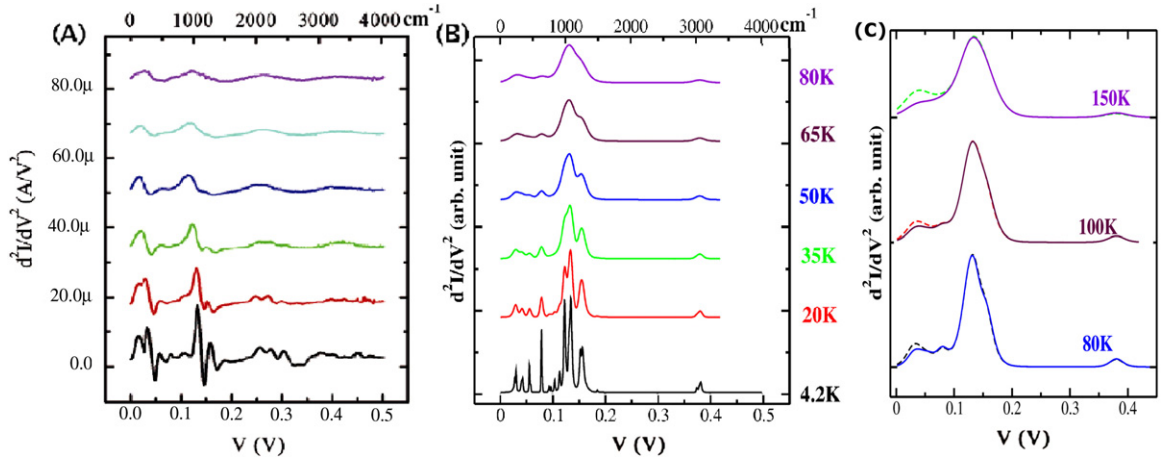

Figure 4. Temperature dependent IETS spectra of the octane dithiol junction from (A) experiment [14] and (B) calculations. The intensity is in arbitrary units. A comparison between calculated spectra with (dashed line) and without (solid line) the factor of thermal population is given in (C).

the calculated I–V curve agrees well with experiment, and all show a very small temperature dependence.

On the other hand, the IETS spectra of the same system show significant temperature dependence as revealed by both experiments [14] and calculations [31]. In figure 4, the experimental and newly calculated spectra are given for a comparison. The agreement between the theory and the experiment is quite good. Both show the same evolution of spectral bands upon the increase of temperature. As an example, in both cases, the peak for mode $\delta(CH_2)$ at 185 mV disappears at 35 K, and the peak for mode $\gamma(CH_2)$ at 155 mV becomes invisible at 50 K. It is noticed that the vibrational features above 80 mV decay relatively faster than those below 80 mV, which could be related to the thermal population since it strongly affects the modes of small frequencies. The calculated temperature dependent IETS spectra with and without the factor of thermal population are shown in figure 4(C). As expected, the temperature effects are mostly introduced by the Fermi distribution. The thermal population has noticeable effects on IETS spectra below 10 mV, and becomes stronger when the temperature increases. The effect of thermal population destroys the one to one correspondence between vibration frequency and IETS peak, and thus complicates the spectral assignments of the IETS. It has a more important, probably positive, implication for computational models that are needed for modeling IETS spectra. It is often argued that one should use as a big gold cluster as possible to model molecular junctions. It is also known that the use of large gold clusters will introduce many vibrational modes with small frequencies, which either come from the metal atoms or from the molecule–metal bonding. In this energy region, thermal population will have considerable effects which will smear out these vibrational features completely and show a broad structure instead. Reliable information about molecular junction can only be extrapolated from the high frequency molecular features.

3.2. Spatial localization

In the energy space, the vibrational motions of a molecule inside the junction are given by the spectral features in an IETS spectrum. At a given energy, the motion of a

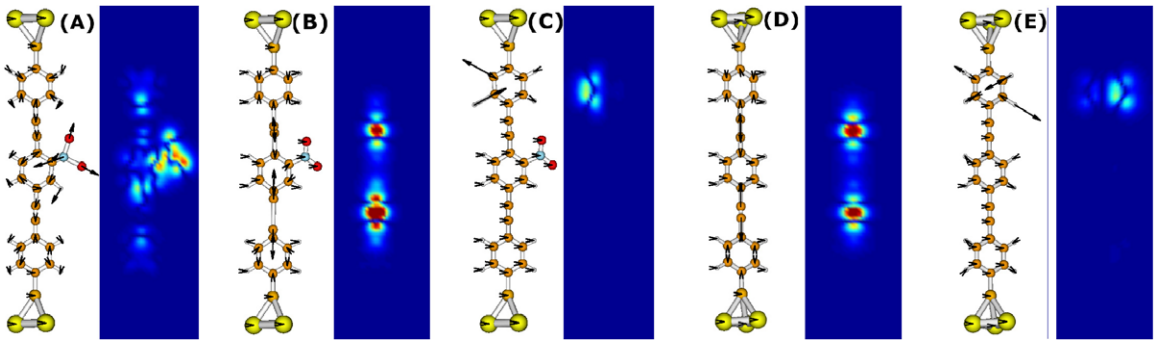

Figure 5. Calculated IETS spatial maps for vibrational modes of the extended molecule Au_3–OPE–NO_2–Au_3 with frequencies (A) 1246.1 cm^{-1}, (B) 2230.7 cm^{-1} and (C) 3202.9 cm^{-1}; and for vibrational modes of the extended molecule Au_3–OPE–Au_3 with frequencies (D) 2227.8 cm^{-1} and (E) 3202.4 cm^{-1}.

molecule that is associated with a particular vibrational mode can be represented in a spatial distribution or an image. Starting with an important experiment by Stipe *et al* [24], IETS with scanning tunneling microscope (STM), IETS-STM has become an established technique for probing the local vibrational density [17–20]. In a recent joint experimental and theoretical study on IETS-STM of the $Gd@C_{82}$ molecule adsorbed on a Ag surface, Grobis *et al* [20] found that the inelastic signal could be spatially localized and detectable only on certain parts of the $Gd@C_{82}$ molecule. In principle our theoretical approach is also capable of providing IETS-STM images of molecular devices. Working with the site representation, one can approximate the intensity of the inelastic signal coupling to vibrational mode Q_a at position $\vec{r}$ as the nuclear motion dependent part of the wavefunction:

$$\sum_K \left\langle \frac{\partial K_0^{\eta}(\vec{r})}{\partial Q_a} Q_a \middle| \Psi(\vec{r}) \right\rangle.$$

We have presented the distributions of small major vibrational modes appearing in IETS spectra of α,ω-bis(thioacetyl)oligophenylenethynylene (OPE) and OPE–NO_2 molecular junctions in figure 5. The image of the vibrational mode at a frequency of 1246.5 cm^{-1} is shown to be mostly localized on the N–O bond. Spatial maps of vibrational modes at frequencies 2233.1 and 3202.5 cm^{-1} of OPE–NO_2 demonstrate very different localization behavior. The same vibrational modes for the pure OPE molecule are presented in figures 5(D) and (E) for comparison. It can be seen that the electron donor group NO_2 makes a negligible contribution to the images of these two vibrational modes. The strong localization of vibrational modes in IETS spectra thus indicate that one should be able to extrapolate pure molecular structure information from the IETS measurements.

3.3. Spectral lines

A spectral line in the IETS spectrum is defined by three parameters: vibrational frequency, scattering intensity and linewidth. Our formulation allows us to provide an accurate description for a spectral line within the harmonic approximation. The best example is the IETS spectrum of an octane dithiol (C8) molecular junction. The alkane chain is

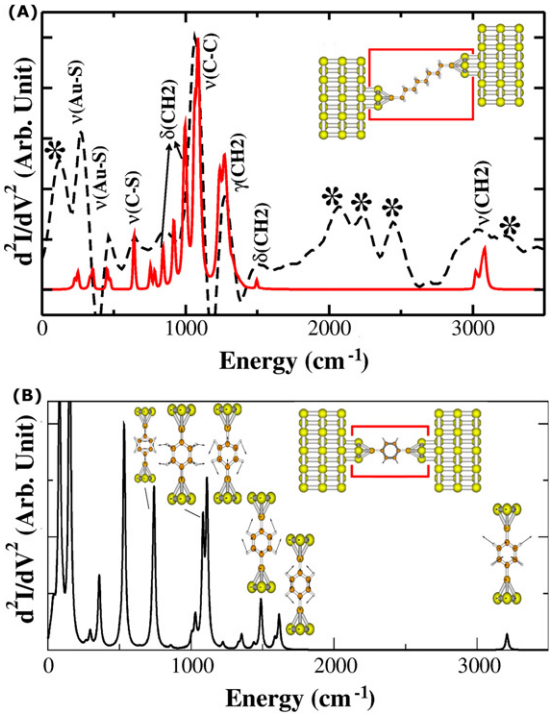

Figure 6. (A) Calculated (solid line) and experimental [14] (dashed line) IETS spectra of an octane dithiol (C8) molecular junction at a working temperature of 4.2 K. Star marks show the background signal in the experiment. (B) Calculated IETS spectrum of a benzene dithiol molecular junction. The corresponding molecular junction models are shown in the insets.

certainly not a good conductor but its stable structure has made it an ideal system for calibrating the experiments of different groups [51–54].

As shown in the inset of figure 6(A), the extended molecule used in the calculations consists of two triangular gold trimers chemically bonded with an octane dithiol (C8) molecule through S–Au bonds. The calculated IETS spectrum of the C8 junction is given in figure 6(A), together with the experimental spectrum of Wang *et al* at a temperature of 4.2 K [14] for comparison. The agreement between theory and experiment is remarkable. Almost all observed molecular peaks in the experimental spectrum have been reproduced.

A detailed spectral assignment can also be provided. For instance, the spectral peak at 1065 cm^{-1} is induced by the stretch of the C–C bond (ν(C–C)), and the peak at 1250 cm^{-1} should be ascribed to the out-of-plane wagging of CH_2 (γCH_2), while the one at 1492 cm^{-1} comes from the scissor motion of CH_2 (δCH_2). Both theoretical and experimental results show that the intensity of the vibronic feature follows the order: ν(C–C)(1065 cm^{-1}) > $\gamma(CH_2)$(1250 cm^{-1}) > $\delta(CH_2)$(1492 cm^{-1}). Calculations have also been able to reveal the structures that were smeared out by the Si_3N_4 substrate in the experiment [14]. Our computational scheme also allows to calculate the spectral linewidth directly, which is determined by the orbital characters and the molecule–metal bonding. For example, the calculated full width at half maximum (FWHM) for the spectral profile of mode ν(C–C) at 1065 cm^{-1} is found to be around 6.1 meV, to be compared with the experimental result of 3.73 ± 0.98 meV [14].

The strong chemical bond between the molecule and the electrodes has resulted in large lifetime broadening of the spectral profile. When physical absorption occurs, the linewidth caused by the lifetime of the conductive vibrational state becomes too small to be detected. In this case, the instrument broadening becomes a dominant factor, giving an uniform width for all spectral lines. We have predicted the high resolution IETS spectrum of a benzene dithiol–gold junction, whose spectral linewidth is limited only by the natural lifetime of each conductive state (see figure 6(B)). The IETS spectrum of the benzene dithiol junction is quite different from that of the octane dithiol junction, which proves yet again the point that the IETS spectrum can be used for the identification of molecules. It should be noted that our formulation does not include effects of the environment, such as thermal baths and substrates, and therefore fails to describe the negative spectral lines observed in the experiments.

3.4. Molecular conformations

Identification of molecules inside the devices has been one of the difficulties in the realization of molecular electronics. The lack of proper experimental tools that could probe or visualize single molecules in a junction has caused many doubts about different experiments. To this end, IETS comes out as a perfect solution since it is directly associated with the vibrations of molecules inside the junctions and can thus be used to verify the existence of molecules inside the junction and hopefully to identify their structures.

A major problem that experimentalists have faced is the lack of control of the molecular confirmation when forming molecular junctions. Even with the same molecule, different confirmations could be obtained. A good description of confirmation dependent IETS should help experimentalists to understand their experiments. For this purpose, theoretical modeling can be essential and helpful. Here we demonstrate how sensitive IETS spectra are to the conformation of the molecule in question.

Again, we have chosen alkane chain molecular junctions as the example. Calculations show that the confirmation of molecule C8 remains planar when it is connected to two

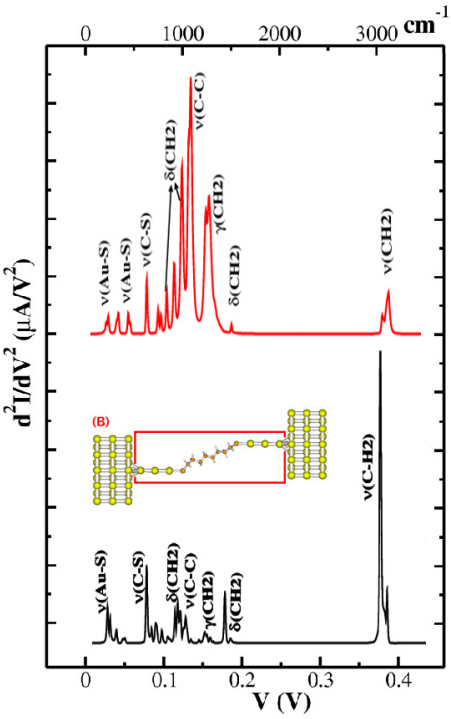

Figure 7. Calculated IETS spectra of octane dithiol (C8) molecular junctions for (A) the Tr1 configuration(red line), and (B) the Ch1 configuration (black line) at the working temperature of 4.2 K.

triangular gold trimers (Tr1 configuration), while it becomes twisted if it is bonded to two gold chains (Ch1 configuration). Such a conformational change has dramatic effects on the appearance of IETS spectra. The calculated IETS spectra for both Tr1 and Ch1 C8 junctions are illustrated in figure 7. It is noted that from the Tr1 configuration to the Ch1 configuration, the highest IETS peak changes from the ν(C–C) mode at 1065 cm^{-1} to the $\delta(CH_2)$ mode at 3081 cm^{-1}. Furthermore, the intensity of the spectral features in the Ch1 configuration follows the order $\delta(CH_2)$ (3081 cm^{-1}) > ν(C–C)(1065 cm^{-1}) > $\gamma(CH_2)$ (1387 cm^{-1}), which is completely different from that for the Tr1 configuration.

Another example is the undecane thiolate (C11, $S(CH_2)_{11}$ H) molecular junction, in which only one side is chemically bonded to the gold electrode. We would like to show that by comparing the experimental result [13] with calculated spectra for a different conformation, one can determine the actual molecular structure inside the junction. And without the help of theoretical modeling, the usefulness of IETS is rather limited. Three different extended molecular systems have been taken into account: (1) C11 with gas phase geometry trapped in triangular gold trimers (Tr1); (2) optimized Tr1 geometry (Tr2); and (3) optimized C11 in linear gold chains (Ch1). The corresponding structures can be found in figure 8, together with the calculated IETS spectra. It can be seen clearly that the simulated spectra are very sensitive to the conformational changes. The most noticeable change of the geometry of C11 in different configurations is the bending of the molecular backbone. It starts with a linear backbone in the Tr1 configuration, becomes slightly bent in the Tr2

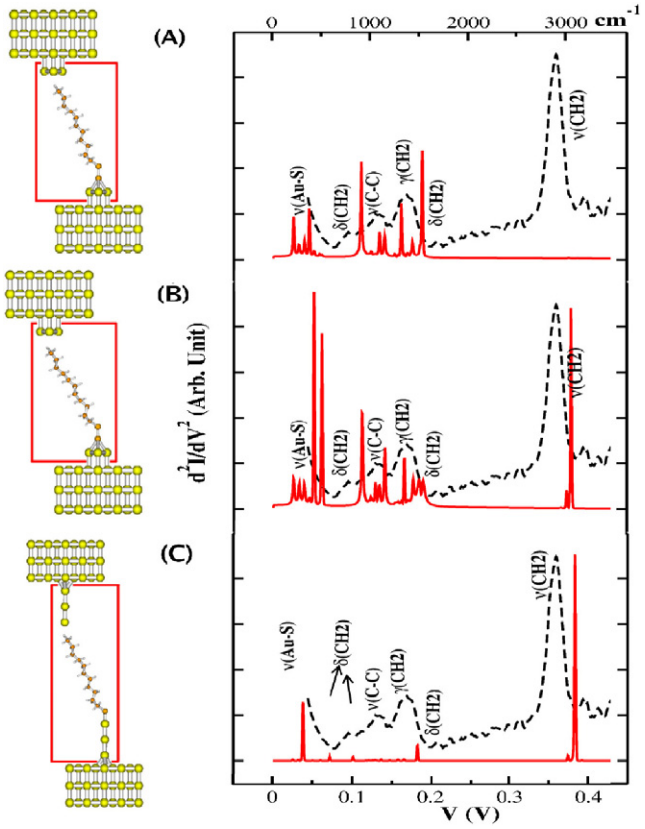

Figure 8. Calculated IETS spectra of undecane thiolate (C11) molecular junctions with (A) Tr1, (B) Tr2 and (C) Ch1 configurations at the working temperature of 4.2 K. The experimental spectrum (dashed line) [13] is also given for comparison. The extended molecular structures are also shown.

configuration, and strongly bend in the Ch1 configuration. The bending of the molecular backbone leads to the enhancement of the spectral peak at 382 mV, corresponding to the $\nu(CH_2)$ mode, and the depression of the remaining spectral features. According to IETS theory [14], molecular vibrations with net dipole moments perpendicular to the interface of the tunneling junction have larger peak intensities than vibrations with net dipole moments parallel to the interface. Thus, it is reasonable that the IETS peaks that come from stretch modes of ν(C–C) and ν(Au–S) are much stronger in spectra of Tr1 and Tr2 than that of Ch1 since the two perpendicular modes in Tr1 and Tr2 configuration are rotated in the bending geometry of Ch1. In comparison with the corresponding experiment [13], one can come to the conclusion that the actual molecular structure in the experimental junction should be in between the configurations of Tr2 and Ch1, and the molecular backbone is definitely bent. It is noted that the experimental spectrum was collected for a molecular monolayer whose linewidth is a summation of a variety of molecular conformations inside the junction.

3.5. Molecule–metal bonding

It is known that an electron's tunneling ability could be heavily affected by the bonding situation between the molecule and metal electrodes. As indicated in equations (8) and (12) for tunneling probability T, the coupling strength V between the electrodes and molecules directly affects the magnitude of the tunneling current and therefore decides the performance of the molecular devices. However, the effect of this parameter is embedded inside the current–voltage characteristics, and it is impossible to extrapolate it from direct conductance measurements. One can note that IETS is also dependent on the electronic structure of the molecular junction around the Fermi level. It should be sensitive to the coupling strength as a result of interaction between frontier molecular orbitals. It is thus possible to apply IETS to determine the coupling strength, or the bond distance between the molecule and the electrodes.

We have calculated IETS spectra for two molecular systems: α,ω-bis(thioacetyl)oligophenylenethynylene (OPE) and α,ω-bis(thioacetyl)oligophenylenevinylene (OPV) sandwiched in gold electrodes. The corresponding extended molecules are shown in figures 9 and 10, respectively. Both molecules are linked to the electrode through the Au–S bonds. A series of bond length (Au–S) dependent IETS spectra for each systems has been calculated. For the case of OPE, the IETS spectrum at the equilibrium marked with zero relative energy and 25.26 Å junction width in figure 9 is used as the reference. It can be seen that the experimental spectrum is largely reproduced except for the features around 275 meV, corresponding to the ν(C≡C) stretch mode. Based on the results for alkane chains, one might suggest that the relatively small intensity of the stretch mode is a result of the strong Au–S chemical bond. By loosening the bonding between the molecule and the electrode, a better agreement between the theory and the experiment indeed emerges. It is also found that the spectral feature at 25 meV cannot be from the molecule itself, but the experimental background. By removing this background, the calculated spectrum for the junction with a width of 25.86 Å should be in very good agreement with the experiment. It is also shown that the OPE molecule is loosely bonded to the gold electrodes. The same observation holds for OPV molecular junctions as the calculated bond length dependent IETS spectra in figure 10 are shown. The best agreement between theory and the experiment for OPV is obtained for the junction a width of 25.7 Å, about 1 Å wider than the equilibrium distance.

3.6. Intermolecular interactions

When a junction is made from a molecular monolayer, the intermolecular interaction could have considerable effects on current–voltage characteristics. Experimental studies on the temperature dependence of electron transport in self-assembled monolayers (SAMs) have indicated that there is a difference in conduction properties between just having a single molecule bridging a junction and having many molecules interact in a SAM [55–57]. It is difficult to control how many molecules can be bonded to electrodes. Imagining a situation where the source and drain electrodes are bonded to different molecules, the tunneling electron injected to one of the molecules thus has to be coupled to another through intermolecular interactions. Based on the current–voltage characteristics alone, it is almost impossible to determine how the molecules are interacting

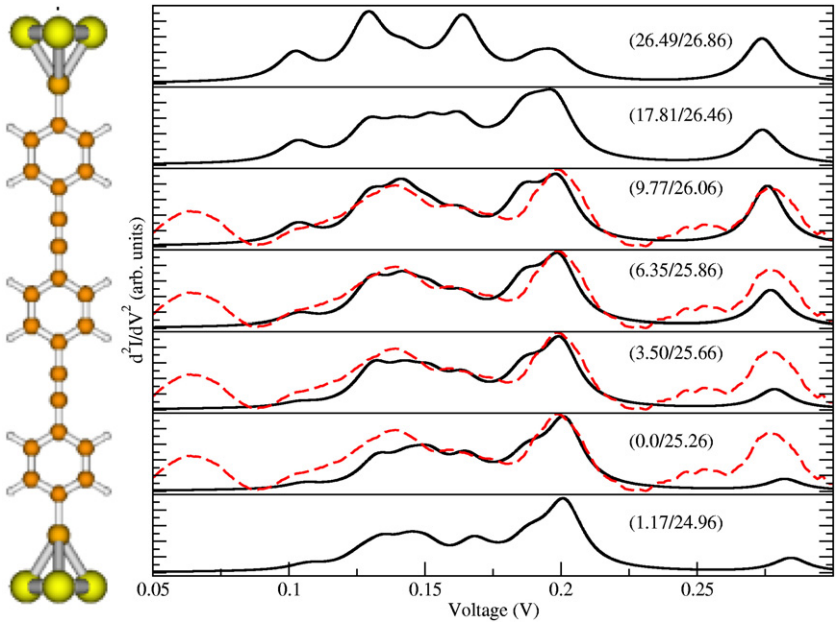

Figure 9. IETS for OPE due to changes in junction distance. Values in parenthesis indicate relative energy in kcal mol^{-1} (left) and junction width in Å (right). The dashed (red) lines represent the experimental IET spectrum.

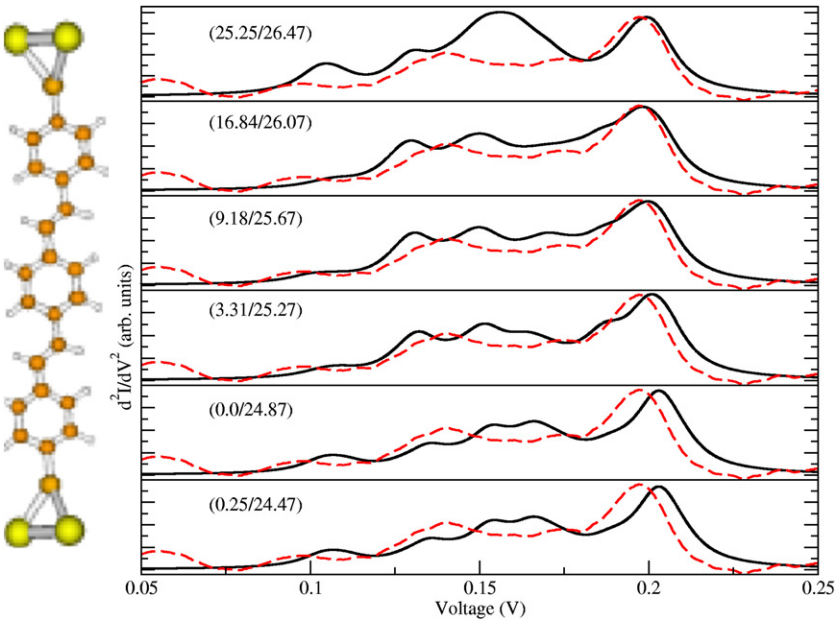

Figure 10. IETS for OPV due to changes in junction distance. Values in parenthesis indicate relative energy in kcal mol^{-1} (left) and junction width in Å (right). The dashed (red) lines represent the experimental IET spectrum.

inside the junction. We have proposed the use of IETS to find out the possible fingerprints of intermolecular interaction [34]. A molecular junction consisting of two benzene dithiol ($S(CH)_6SH$) molecules has been studied.

The IETS spectrum of a single benzene dithiol molecule in a gold junction is also calculated for reference (see figure 11(A)). In this case, one molecule is bonded with two electrodes through Au–S bonds. It is noted that strong IETS peaks seem to be related to the vibrational modes possessing components perpendicular to the metal–molecule interfaces, such as the peaks labeled with 1 and 4 in figure 11(A), while the modes consisting of out-of-benzene plane motions make small contributions to the IET signals. To examine the effect of intermolecular interaction, we have constructed three model systems, consisting of a pair of benzene dithiol molecules with three different mutual orientations: side overlapping (SO), partial overlapping (PO) and complete overlapping (CO). In all three models, one molecule is chemically bonded to only one electrode. The corresponding conformations and spectra are shown in figures 11(B)–(D), respectively. In all cases, the

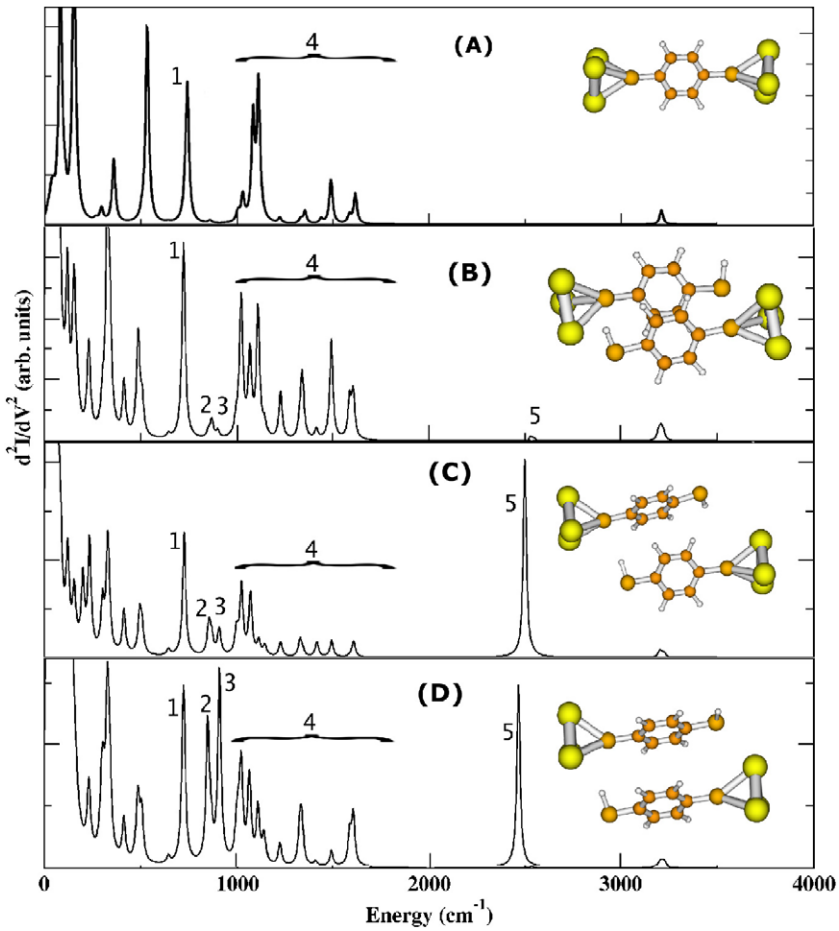

Figure 11. Calculated IETS spectra for junctions consisting of (A) a single benzene dithiol; and a pair of benzene dithiolate molecules separated by a distance of 3.6 Å in three different interacting modes: (B) side overlapping, (C) partial overlapping, and (D) complete overlapping. Inset pictures represent conformations of extended molecules.

intermolecular distance between two benzene rings is set to be 3.6 Å.

In comparison with the spectrum of a single molecule, the interacting molecular pair leads to more spectral features. For instance, the new peaks 2 and 3 in figure 11(B) are out-of-plane wagging modes that are not presented in figure 11(A). It is noted that going from SO to PO and CO configurations, spectral peaks 2 and 3 become even stronger. This is certainly related to the degree of overlap between two benzene rings, which lead to stronger intermolecular interaction and to enhanced performance of out-of-plane wagging modes. There is another noticeable extra IETS peak, labeled as 5 in figures 11(B)–(D), appearing in the spectra of molecular pairs. It comes from the S–H stretching mode, which is absent in the single benzene dithiol system. Calculations have also shown that if there is enough overlap with the S–H stretching and the opposite contact, the characteristic S–H stretching peak 5 will be strong. However, the absence of the S–H stretching mode for the side overlapping system shows that looking for this peak in the IETS spectra alone is not enough to determine whether an experimental system has successfully formed bonds at both ends or not. It is important to take into account the change in the overall spectral profile with respect to different intermolecular interactions, for which accurate theoretical modeling is always needed.

4. Conclusions

In recent years, one has witnessed a rise in the use of IETS due to the fact that it might be the only experimental technique that is able to provide information about single molecules inside molecular junctions. The complicated spectral features could sometimes be understood by certain propensity rules [26]. However, as demonstrated in this work, the IETS spectrum is very sensitive to small conformational changes, intermolecular interaction and the molecule–metal bond length. It is thus essential to have the assistance of theoretical modeling. Our recently developed quantum chemical approach could be a useful theoretical tool to go hand-in-hand with experiments. It has been able to reproduce many experimental spectra with good accuracy, and to relate the spectral changes to microscopic properties of molecules inside the junctions. The current formulation of our approach has also provided a good platform for future development, for instance the inclusion of electron resonances, charging effects and dynamics.

Acknowledgments

This work is supported by the Swedish Research Council (VR), the Carl Trygger Foundation (CTS) and the Swedish National Infrastructure for Computing (SNIC).

References

[1] Aviram A and Ratner M A 1974 *Chem. Phys. Lett.* **29** 277
[2] Joachim C, Gimzewski J K and Aviram A 2000 *Nature* **408** 541
[3] Nitzan A and Ratner M A 2003 *Science* **300** 1384
[4] Hänggi P, Ratner M A and Yaliyaki S (ed) 2002 *Chem. Phys.* **281** 111–502 (special issue)
[5] Reed M A 2004 *Nat. Mater.* **3** 286
[6] Reed M A, Zhou C, Muller C J, Nurgin T P and Tour J M 1997 *Science* **278** 252
[7] Wang W Y, Lee T and Reed M A 2005 *Rep. Prog. Phys.* **68** 523
[8] Ventra M D, Pantelides S T and Lang N D 2000 *Phys. Rev. Lett.* **84** 979
[9] Brandbyge M, Mozos J-L, Ordejon P, Taylor J and Stokbro K 2002 *Phys. Rev.* B **65** 165401
[10] Taylor J, Guo H and Wang J 2001 *Phys. Rev.* B **63** 245407
[11] Haug H and Jauho A P 1996 *Quantum Kinetics in Transport and Optics of Semiconductors* (Berlin: Springer)
[12] Mujica V, Kemp M and Ratner M A 1994 *J. Chem. Phys.* **101** 6849
[13] Kushmerick J G, Lazorcik J, Patterson C H, Shashidhar R, Seferos D S and Bazan G C 2004 *Nano Lett.* **4** 639
[14] Wang W, Lee T, Kretzschmar I and Reed M A 2004 *Nano Lett.* **4** 643
[15] Yu L H, Keane Z K, Ciszek J W, Cheng L, Stewart M P, Tour J M and Natelson D 2004 *Phys. Rev. Lett.* **93** 266802
[16] Yu L H, Zangmeister C D and Kushmerick J G 2006 *Nano Lett.* **6** 2515
[17] Heinrich A J, Gupta J A, Lutz C P and Eigler D M 2004 *Science* **306** 466
[18] Hirjibehedin C F, Lutz C P and Heinrich A J 2006 *Science* **312** 1021
[19] Vitali L *et al* 2004 *Phys. Rev. Lett.* **93** 136103
[20] Grobis M *et al* 2005 *Phys. Rev. Lett.* **94** 136802
[21] Pascual J I, Jackiw J J, Song Z, Weiss P S, Conrad H and Rust H-P 2001 *Phys. Rev. Lett.* **86** 1050
[22] Park H, Park J, Lim A K L, Anderson E H, Alivisatos A P and McEuen P L 2000 *Nature* **407** 57
[23] Osorio E A, O'Neill K, Stuhr-Hansen N, Nielsen O F, Bjørnholm T and van der Zant H S J 2007 *Adv. Mater.* **19** 281
[24] Stipe B C, Rezaei M A and Ho W 1998 *Science* **280** 1732
[25] Troisi A, Ratner M A and Nitzan A 2003 *J. Chem. Phys.* **118** 6072
[26] Troisi A and Ratner M A 2006 *J. Chem. Phys.* **125** 214709
[27] Galperin M, Ratner M A and Nitzan A 2004 *Nano Lett.* **4** 1605
[28] Troisi A and Ratner M A 2005 *Phys. Rev.* B **72** 33408
[29] Chen Y-C, Zwolak M and Ventra M Di 2004 *Nano Lett.* **4** 1709
[30] Chen Y-C, Zwolak M and Ventra M Di 2005 *Nano Lett.* **5** 621
[31] Jiang J, Kula M, Lu W and Luo Y 2005 *Nano Lett.* **5** 1551
[32] Jiang J, Kula M and Luo Y 2006 *J. Chem. Phys.* **124** 034708
[33] Kula M, Jiang J and Luo Y 2006 *Nano Lett.* **6** 1693
[34] Kula M and Luo Y 2008 *J. Chem. Phys.* **124** 064705
[35] Paulsson M, Frederiksen T and Brandbyge M 2006 *Nano Lett.* **6** 258
[36] Ness H 2006 *J. Phys.: Condens. Matter* **18** 6307
[37] Maddox J B, Harbola U, Liu N, Silien C, Ho W, Bazan G C and Mukamel S 2006 *J. Phys. Chem.* A **110** 6329
[38] Sergueev N, Demkov A A and Guo H 2007 *Phys. Rev.* B **75** 233418
[39] Yaliraki S N, Kemp M and Ratner M A 1999 *J. Am. Chem. Soc.* **121** 3428
[40] Samanta M P, Tian W, Datta S, Henderson J I and Kubiak C P 1996 *Phys. Rev.* B **51** R7626
[41] Damle P S, Ghosh A W and Datta S 2001 *Phys. Rev.* B **64** 201403
[42] Su W Y, Jiang J and Luo Y 2005 *Chem. Phys. Lett.* **412** 406
Jiang J, Lu W and Luo Y 2004 *Chem. Phys. Lett.* **400** 336
Wang C K and Luo Y 2003 *J. Chem. Phys.* **119** 4923
[43] Galperin M, Ratner M A and Nitzan A 2007 *J. Phys.: Condens. Matter* **19** 103201
[44] Landauer R 1957 *IBM J. Res. Dev.* **1** 223
Landauer R 1970 *Phil. Mag.* **21** 863
[45] Wang C K, Fu Y and Luo Y 2001 *Phys. Chem. Chem. Phys.* **3** 5017
[46] Feynman R P 1972 *Staticstical Mechanics* ABP (Reading, MA: Addison-Wesley) pp 286–9
[47] Jiang J and Luo Y 2006 *QCME-V1.0 (Quantum Chemistry for Molecular Electronics)* (Sweden: Royal Institute of Technology)
[48] Becke A D 1993 *J. Chem. Phys.* **98** 5648
[49] Hay P J and Wadt W R 1985 *J. Chem. Phys.* **82** 270
Wadt W R and Hay P J 1985 *J. Chem. Phys.* **82** 284
Hay P J and Wadt W R 1985 *J. Chem. Phys.* **82** 299
[50] Frisch M J *et al* 2003 *Gaussian 03, Revision A.1* (Pittsburgh, PA: Gaussian)
[51] Holmlin E, Haag E, Chabinyc M L, Ismagilov R F, Cohen A E, Terfort A, Rampi M A and Whitesides G M 2001 *J. Am. Chem. Soc.* **123** 5075
[52] Wold D J, Haag R, Rampi M A and Frisbie C D 2002 *J. Phys. Chem.* B **106** 2813
[53] Cui X D, Zarate X, Tomfohr J, Sankey O F, Primak A, Moore A L, Moore T A, Gust D, Harris G and Lindsay S M 2002 *Nanotechnology* **13** 5
[54] Wang W, Lee T and Reed M A 2003 *Phys. Rev.* B **68** 035416
[55] Selzer Y, Cabassi M A, Mayer T S and Allara D L 2004 *J. Am. Chem. Soc.* **126** 4052
[56] Selzer Y, Cabassi M A, Mayer T S and Allara D L 2004 *Nanotechnology* **15** S483
[57] Selzer Y, Cai L, Cabassi M A, Yao Y, Tour J M, Mayer T S and Allara D L 2005 *Nano Lett.* **5** 61